


Article

Dry Printing of Ag–Ni Conductive Particles Using Toner-Type Printed Electronics

Fumiya Sawamura¹, Chen Yi Ngu¹, Raiki Hanazaki¹, Kaito Kozuki¹, Sayaka Kado², Masatoshi Sakai^{1,*} 
and Kazuhiro Kudo¹

¹ Department of Electrical and Electronic Engineering, Chiba University, Chiba 263-8522, Japan;

² Center for Analytical Instrumentation, Chiba University, Chiba 263-8522, Japan

* Correspondence: sakai@faculty.chiba-u.jp

Abstract: Printed electronics are a set of additive manufacturing methods for creating future flexible electronics on thin polymeric sheets. We proposed the toner-type, dry, page-printing of Ag–Ni composite conductive particles on flexible plastic sheets without pre-treatment. No chemical solvents are necessary to compose the inks of the electronic materials used for the toner-type printing, and no chemical treatment is required for the plastic film substrate surface. In addition, multilayer printing is simple when using toner printing because previously printed materials do not need to be resolved; furthermore, composing the thick films of the electronic materials is relatively simple. In this study, we fabricated an Ag–Ni composite toner to improve the fluidity of the toner particles compared to bare Ag particles. We successfully printed IC peripheral circuits at a resolution of 0.20 mm and demonstrated that the actual electrical circuit pattern can be formed using our method.

Keywords: printed electronics; flexible electronics; additive manufacturing; conductive nanoparticle



Citation: Sawamura, F.; Ngu, C.Y.; Hanazaki, R.; Kozuki, K.; Kado, S.; Sakai, M.; Kudo, K. Dry Printing of Ag–Ni Conductive Particles Using Toner-Type Printed Electronics. *Appl. Sci.* **2022**, *12*, 9616. <https://doi.org/10.3390/app12199616>

Academic Editor: Abílio Manuel Pinho de Jesus

Received: 30 August 2022

Accepted: 22 September 2022

Published: 25 September 2022

Publisher's Note: MDPI stays neutral with regard to jurisdictional claims in published maps and institutional affiliations.



Copyright: © 2022 by the authors. Licensee MDPI, Basel, Switzerland. This article is an open access article distributed under the terms and conditions of the Creative Commons Attribution (CC BY) license (<https://creativecommons.org/licenses/by/4.0/>).

1. Introduction

Flexible and printed electronics are the next-generation technologies that will lead to paper-like electronic devices, such as healthcare sensors, flexible handheld devices, displays, and various wearable electronic devices. Printed electronics are also valuable owing to the material savings resulting from their additive nature [1–28]. Conventional semiconductor device technologies include subtractive technologies, such as etching, photolithography, and dicing. In contrast, various printed electronics methods are additive and have material-saving properties, in addition to being disposable by using naturally decomposed electronic materials for the inks [29–32]. Prototyping and the subsequent manufacturing of a wide variety of products in small quantities is an advantage of the on-demand printing technique. Ink-jet printing is an on-demand printing method that is sufficiently developed globally. Electrophotographic printing is another on-demand printing method that uses toner particles instead of inks [33,34]. The conductive toner particles used in our electrophotographic printed electronics are almost entirely bare metal particles that do not include chemical agents in the liquid inks and improve the solubility and viscosity. Therefore, a high-temperature thermal treatment after printing was unnecessary. Moreover, because our method uses metal particles instead of a solvent for creating the inks, re-dissolution of the pre-printed pattern by the solvent of the next layer does not occur. Namely, multilayer printing is easily achieved using this method. Chemical vapor does not volatilize after printing; therefore, extra time is not required for the printed pattern to dry, leading to a high throughput. In addition, the advantage of electrophotographic printing, which contributes to the high throughput, is that this method is based on page-printing and not dot-printing. Page-printing ensures the printing of electrical circuits with a high throughput, in which mm to μm scale patterns coexist. Printing of the mm (PCB level) to the μm scale (intra-IC circuit pattern) with a coexisting pattern is necessary to enable future electronics to be entirely printed.

This study demonstrates that the IC peripheral pattern can be fabricated using electrophotographic printing with Ag–Ni composite toner particles, which consist of Ag particles and Ni nanoparticles surrounding the Ag particles. Ni nanoparticles prevent the natural aggregation of Ag particles and maintain the fluidity of the conductive toner particles. In addition, compressed Ag–Ni toner particles have been demonstrated to exhibit a low electrical resistivity of $6.89\text{--}9.43 \times 10^{-8} \Omega\cdot\text{m}$, which was approximately two times higher than that of the compressed bare Ag particles, and were comparable to the electrical resistivity of bulk Ni.

2. Materials and Methods

Ag micro-powder particles with a nominal diameter of 2–3.5 μm (Sigma-Aldrich Co. LLC, St. Louis, MO, USA) were used in this study. Ni nanopowder particles with a nominal diameter of ~ 150 nm were used in the Ag–Ni composite toner (Sigma-Aldrich Co. LLC). Several commercially purchased micro- and nanoparticles are naturally aggregated; as a result, the actual diameter of these particles was generally larger than the reported nominal diameters. Therefore, before use, the naturally aggregated Ni particles were ball-milled to retain the original fine nanoparticles. Conversely, the Ag microparticles were used as purchased and were not milled because Ag is significantly soft; thus, milling would promote Ag aggregation. The Ag:Ni weight ratio in the Ag–Ni composite particles was 5:1. The volume ratio was Ag:Ni = 1:0.236. The role of the Ni particles is to prevent the natural aggregation of the conductive toner. Therefore, this ratio satisfies the required Ni composition and is not too sensitive to be used as a conductive toner. An excessive amount of Ni would lead to an increase in the electrical resistivity of the conductive toner after sintering. The Ag micro-powder and Ni nanopowder were gently mixed, obtaining Ag–Ni composite toner particles.

Figure 1a,b demonstrate the repose angle estimation for Ag and Ag–Ni conductive particles. The higher repose angle for the Ag particles ($72\text{--}85^\circ$) shown in Figure 1a compared to that of the Ag–Ni particles ($54\text{--}75^\circ$) shown in Figure 1b indicates that the bare Ag particles have lower fluidity compared to that of the Ag–Ni particles, owing to the higher natural aggregation between bare Ag particles. Therefore, the Ni particles distributed on the surface of the Ag particles inactivated the Ag–Ni surface and prevented the aggregation of the conductive toner particles. As a result, the particle size distribution was apparently different for the bare Ag and Ag–Ni particles, as shown in Figure 1c,d. Figure 1c,d demonstrate Ag and Ag–Ni particle size distributions that were analyzed using an optical micrograph and image processing software (ImageJ [35,36]), respectively. Figure 1c indicates that the Ag particle size distribution has a peak diameter of approximately 7 μm . Although the nominal particle diameter reported by the manufacturer was 2–3.5 μm , the Ag particles became larger, owing to the natural aggregation demonstrated. In contrast, the Ag–Ni composite particles presented different size distributions, and a lower-side tail and sub-peak appeared at approximately 3 μm , which indicates that the addition of the Ni particles effectively prevented the natural aggregation of the Ag particles.

Figure 2a presents an SEM image of a Ag–Ni conductive particle. Ag and Ni particles are difficult to distinguish based on their appearance. However, the energy-dispersive X-ray spectroscopy of this particle revealed the elemental distribution of the composite particles. Figures 2b,c demonstrate the mapping of the Ag $K\alpha$ X-ray detected points and that of Ni- $K\alpha$, respectively. The Ag $K\alpha$ distribution reflects the entire particle shape ($\sim 5 \mu\text{m}$), as shown in Figure 2a. In contrast, the Ni $K\alpha$ signal distribution indicates that the Ni particles are smaller ($< 1 \mu\text{m}$) and they stick to the surface of the larger Ag particles. If we carefully examine the SEM image after Ag, Ni, and the superimposed EDX image in Figure 2d, it is possible to distinguish Ni and Ag by the brightness in the SEM image. The dark gray particles are the Ni particles that cover the entire surface, while Ag is the bright region slightly observed among the Ni particles. The apparent difference in brightness in the SEM images is due to the secondary electron emission probability between Ag and Ni. As

a result, it was confirmed that the surfaces of the Ag particles were covered with Ni particles.

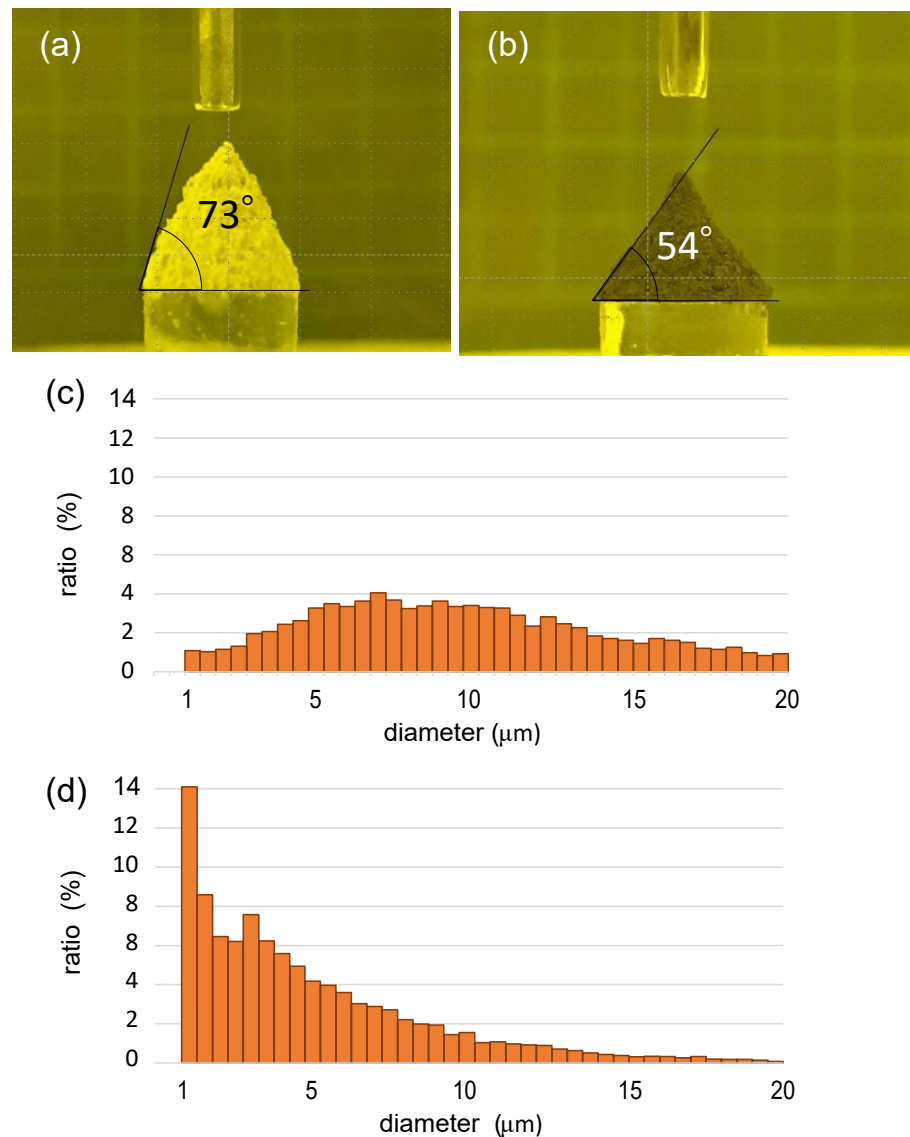


Figure 1. Photograph of the repose angle estimation for Ag toner particles (a) and Ag–Ni composite particles (b). Histogram of the particle size distribution for the bare Ag particles (c) and Ag–Ni composite particles (d), respectively.

In this study, we demonstrated the effectiveness of the Ag–Ni toner particles for printed electronics, owing to their enhanced fluidity and comparable electrical resistivity with bare Ag toner particles. A high fluidity is advantageous for high-resolution patterning. The patterning performance is exhibited by the fabrication of an IC peripheral circuit by using primitive toner printing equipment, as indicated later in Figure 5. To achieve a high contrast and high-resolution printing, both attractive and repulsive electric fields for the toner particles were applied during development. The 4-probe electrical resistivity measurement was conducted to evaluate the resistivity of the compressed Ag–Ni test piece.

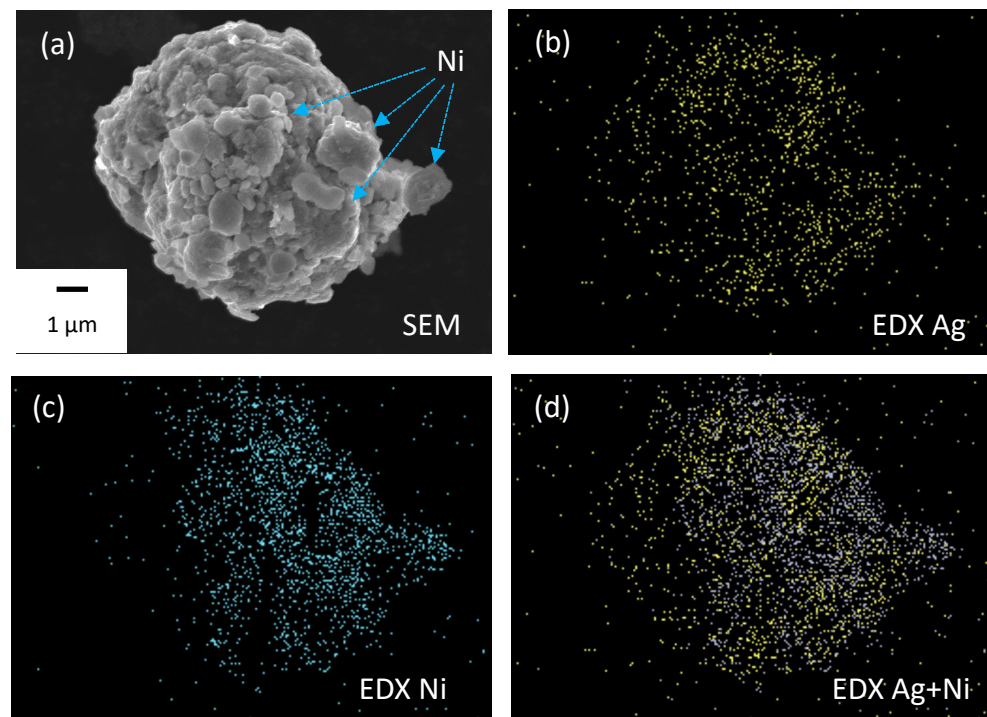


Figure 2. (a) Scanning electron microscopy (SEM) image of a Ag–Ni composite toner particle. (b) Energy dispersive X-ray spectroscopy (EDX) image of the Ag $K\alpha$ X-ray emission distribution, EDX image of the Ni $K\alpha$ X-ray emission distribution (c), and superimposed EDX image of the Ag and Ni EDX $K\alpha$ emission(d).

3. Results

Figure 3 demonstrates an SEM image of the developer used for conductive toner printing. Toner printing uses a developer, which is a mixture of the toner and carrier particles. The small ($<5\ \mu\text{m}$) and bright gray particles are the Ag–Ni conductive toner particles, while the large ($\sim 40\ \mu\text{m}$) and dark gray particles are the carrier particles. Toner particles were distributed on the surface of the carrier particles. The conductive Ag–Ni particles sufficiently adhere to the carrier particle surface, owing to an image force between a charged Ag–Ni particle and carrier particle [34]. The toner and carrier weight ratio in the developer was 1:40. The toner particles were transferred from the carrier particle surface onto the plastic film substrate by applying an external electrostatic force during the printing process. In contrast, carrier particles (P-02 standard carrier, distributed by the Imaging Society of Japan, Tokyo, Japan) consist of a magnetic material and help the toner particles disperse, remain stable in air, and form a magnetic brush structure (shown in Figure 5b later), which are necessary for toner printing. Therefore, the carrier particles remain on the developer and are not transferred to the plastic substrate film.

Figure 4a presents a schematic illustration of the electrostatic potential distribution formed on the PET film surface. The PET film was back-coated with an Al thin film and placed on the charging equipment; the gradation pattern of the electrostatic potential on the PET surface was formed, as illustrated in Figure 4a. The arrangement of the electrical potential on the positively charged PET film was 0, +100, +80, +60, +40, and +20 V from left to right, and that on the negatively charged PET film was 0, −100, −80, −60, −40, and −20 V. We developed the Ag–Ni toner particle on the PET film using primitive electrophotographic printing equipment, which was the same as that depicted in Figure 5. The results of the development of the positively charged PET surface are shown in Figure 4b, which demonstrates that a thin Ag–Ni toner particle was distributed in the 0 V region. However, fewer Ag–Ni particles were distributed in the positively charged region. Moreover, the Ag–Ni particles were effectively repelled in the high-electrical-potential region. Conversely, as shown in Figure 4c, dense Ag–Ni particles were distributed in the

negatively charged region compared to the 0 V region, and the gradation of the Ag–Ni particle density changed from the -20 V to -100 V region. Therefore, Ag–Ni particles were effectively attracted to the lower electric potential region. These results clearly demonstrate that Ag–Ni particles mixed and frictionally charged with the P-02 carrier particles have a net positive charge. Therefore, it is possible to attract and repel conductive Ag–Ni particles using the polarity of an applied external electric field.

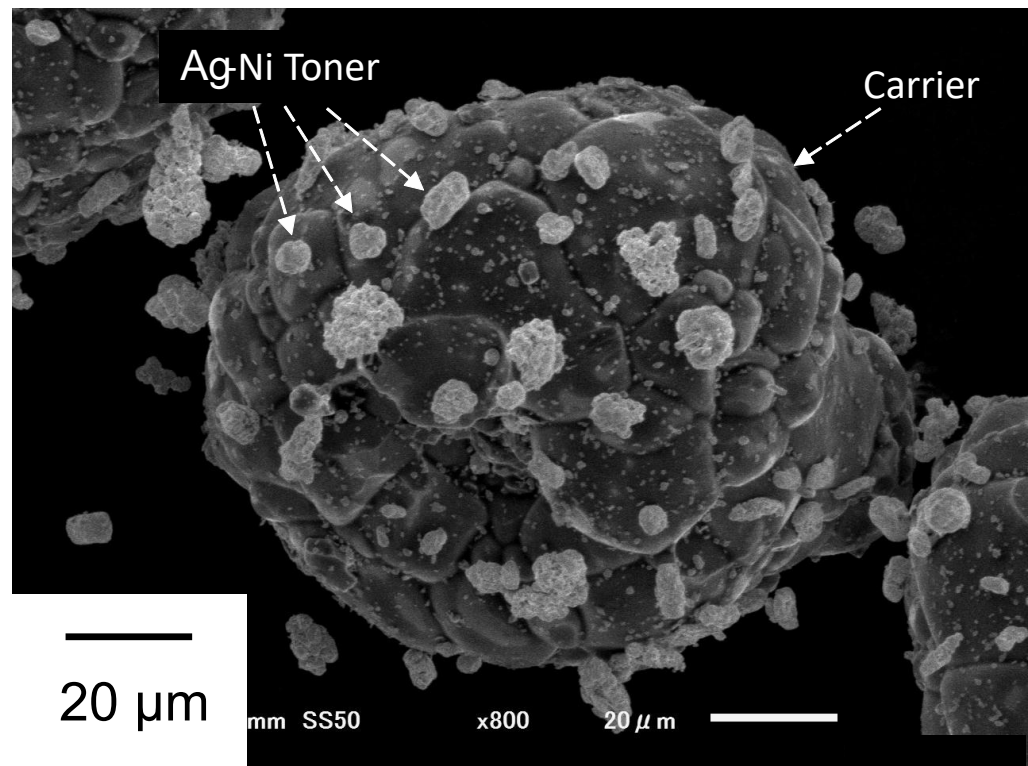


Figure 3. SEM image of the developer comprising a P-02 carrier particle and Ag–Ni composite toner particles.

Figure 5a demonstrates the schematic of the primitive electrographic printing equipment. The developer, comprised of the toner and carrier particles, is loaded into the developer reservoir, which consists of a non-magnetic metal plate. The magnet row moving in a reciprocating motion below the developer reservoir forms the magnetic brush of the developer particle along the magnetic lines of the force, as shown in Figure 5b. An insulator plate with a target electrode and counter electrode was placed above the developer reservoir, and external development and counter electric fields were applied during development. The attractive electric field was applied between the developer reservoir and target electrode, thus the toner particle was attracted to the target electrode by an electrostatic force when the magnetic brush of the developer passed just below the target electrode pattern. During the development of the toner particles, the carrier particles remained on the developer reservoir owing to the attractive magnetic force of the magnets. In contrast, a repulsive electric field was applied between the counter electrode and magnetic brush to inhibit the adhesion of the toner particle to the exterior of the target pattern. The strength of the repulsive electric field was sufficiently weaker than that of the attractive electric field; therefore, the repulsive electric field only inhibits the adhesion of stray toner particles.

Figure 6a demonstrates a photograph of the IC peripheral circuit pattern formed on a polymer film surface using our toner printing method. The applied external voltage in the target pattern was -100 V, and that in the counter electrode was $+50$ V. An external voltage of -100 V was applied to attract the positively charged Ag–Ni toner particles. In contrast, an external voltage of $+50$ V was applied to inhibit the adhesion of the stray Ag–Ni particles. Using these two external electric fields, the high-contrast printing of the fine and

complicated IC peripheral circuits was achieved. Ag–Ni conductive toner particles are observed as a bright line pattern in this picture and form a circuit pattern with sufficient density. The IC peripheral circuit has a 0.20 mm resolution line pattern. This resolution is comparable to that of the current industrial electronics circuit board. Figure 6b presents a magnified view of the Ag–Ni particle pattern, indicated by the broken white rectangle in Figure 6a. The Ag–Ni particles are dispersed on the surface of the polymer film and form circuit patterns by applying an external electrostatic force. The density of the Ag–Ni toner particles in the line pattern varied by the strength of the external electrostatic force. As shown in Figures 4 and 6, a thick deposition of the toner particles in a single development is possible using this method, which is the advantage of the toner-type page printing. In contrast, dot-printing methods require a significant amount of time to create thick patterns in both the plane and thickness directions because several drops of ink are necessary for filling a thick pattern. Toner-type printing enables a wide range of controllability of the thickness in creating an electrical circuit, in which circuit patterns ranging from the μm to cm scale coexist.

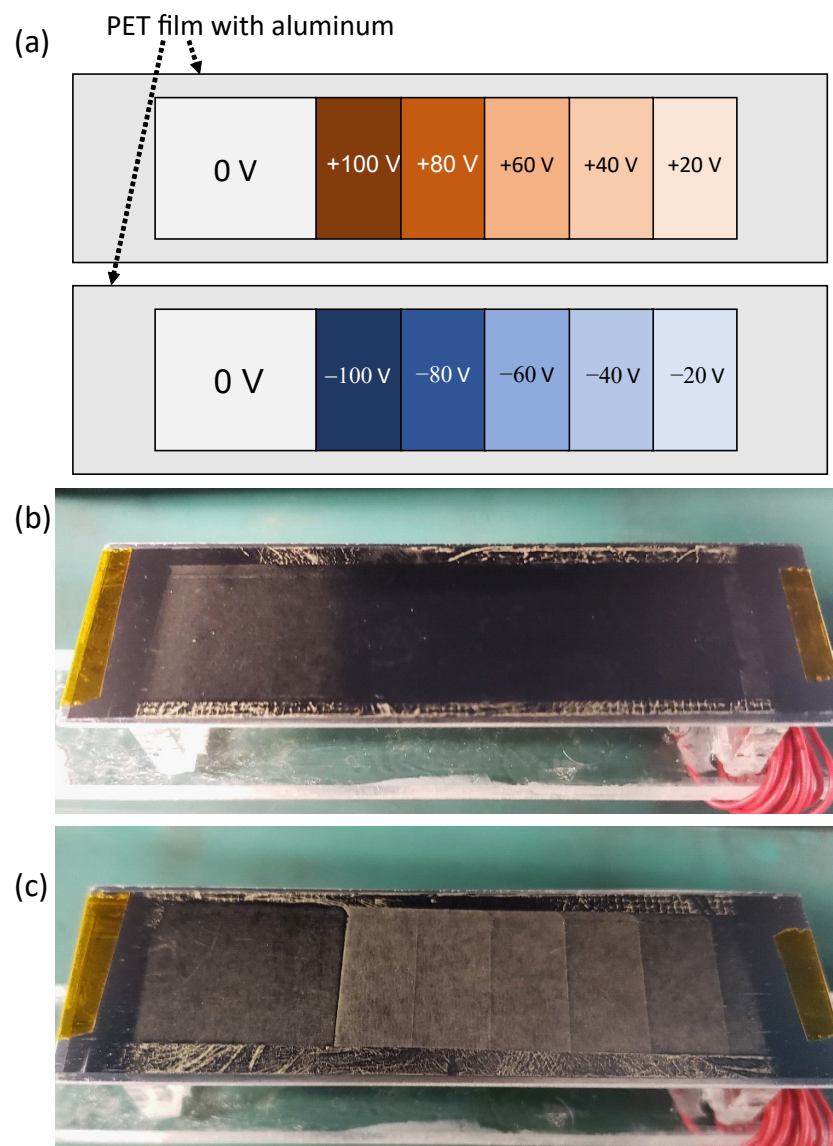


Figure 4. (a) Schematic illustration of the gradation electrostatic potential applied on the PET film. (b) Photograph of the developed Ag–Ni toner pattern on the positive gradation-charged PET surface. (c) Photograph of the developed Ag–Ni toner pattern on the negative gradation-charged PET surface.

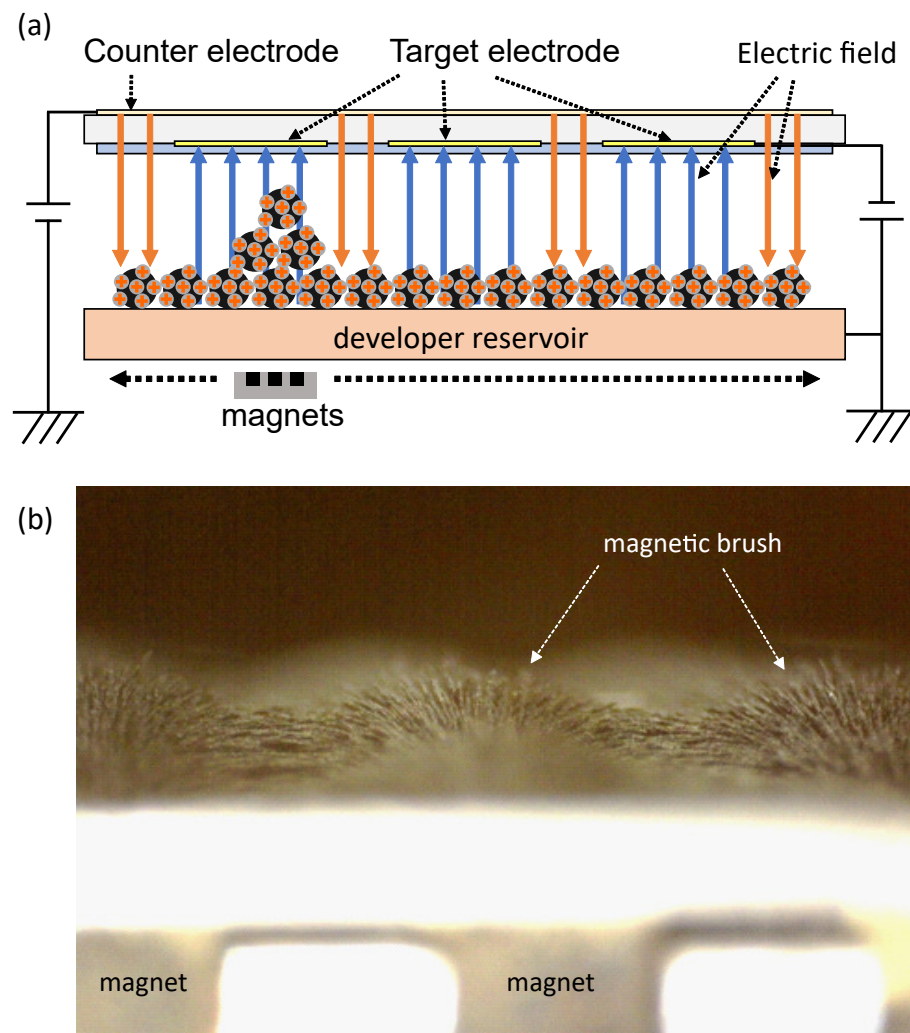


Figure 5. (a) Schematic illustration of the electrophotographic printing equipment. The developer particle, comprised of the toner and carrier, forms a magnetic brush structure along the magnetic lines of the force, and the magnets move in a reciprocating motion by a motorized mechanism. (b) Photograph of the magnetic brush formed in the developer reservoir.

To evaluate the electrical resistance of the Ag–Ni composite circuit, we performed a 4-probe electrical measurement on the compressed test piece. Figure 7a,b demonstrate the Ag and Ag–Ni composite test pieces, respectively, which were molded using oil-press equipment and cut, as shown in Figure 7a,b. Both powders were compressed and exhibited a sufficient stiffness. The Ag-compressed test piece is bright gray and partly shows a metallic luster. In contrast, the Ag–Ni composite test piece is dark gray, similar to the original particle, as shown in Figure 1b. In the Ag–Ni composite particles, Ni nanoparticles on the Ag surface inhibit Ag–Ag aggregation. However, under compression, the Ni particles, which are a minority of the volume, are incorporated between compressed and deformed Ag particles. As a result, the Ag–Ni test piece has the same range of stiffness as the Ag test piece. The electrical resistance measurements were obtained using a 4-probe prober, as shown in Figure 7c. The obtained electrical resistivity of the Ag–Ni composite test piece was $6.89\text{--}9.43 \times 10^{-8} \Omega\cdot\text{m}$. However, the electrical resistivity of the Ag test piece was $3.41\text{--}4.52 \times 10^{-8} \Omega\cdot\text{m}$. The estimated electrical resistivity of the Ag–Ni composite test piece was approximately twice that of the Ag test piece. Furthermore, the electrical resistivities of Ag and bulk Ni were $1.59 \times 10^{-8} \Omega\cdot\text{m}$ and $6.99 \times 10^{-8} \Omega\cdot\text{m}$, respectively. Therefore, the obtained resistivity of the Ag–Ni composite was comparable to that of the bulk Ni. Because the volume ratio of Ag in the Ag–Ni composite particles was approximately 80.9% and Ag is a soft metal that can be easily deformed [37–46], compressed Ag–Ni particles formed direct

Ag–Ag connection networks by being crushed and deformed under sufficient compression. As a result, a relatively low electrical resistivity was achieved, even in only the compressed Ag–Ni particles. This value is sufficiently low compared to other printing methods using ink. Printed electronic circuits using inks present a higher electrical resistivity owing to the residual chemical agents included. To remove the chemical components, the printed pattern should be thermally annealed at a temperature range of near or over 200 °C, where the plastic film substrates that endure this process are limited. Therefore, the Ag–Ni composite toner is expected to be a conductive toner material with sufficient fluidity and high conductivity for toner-type printing.

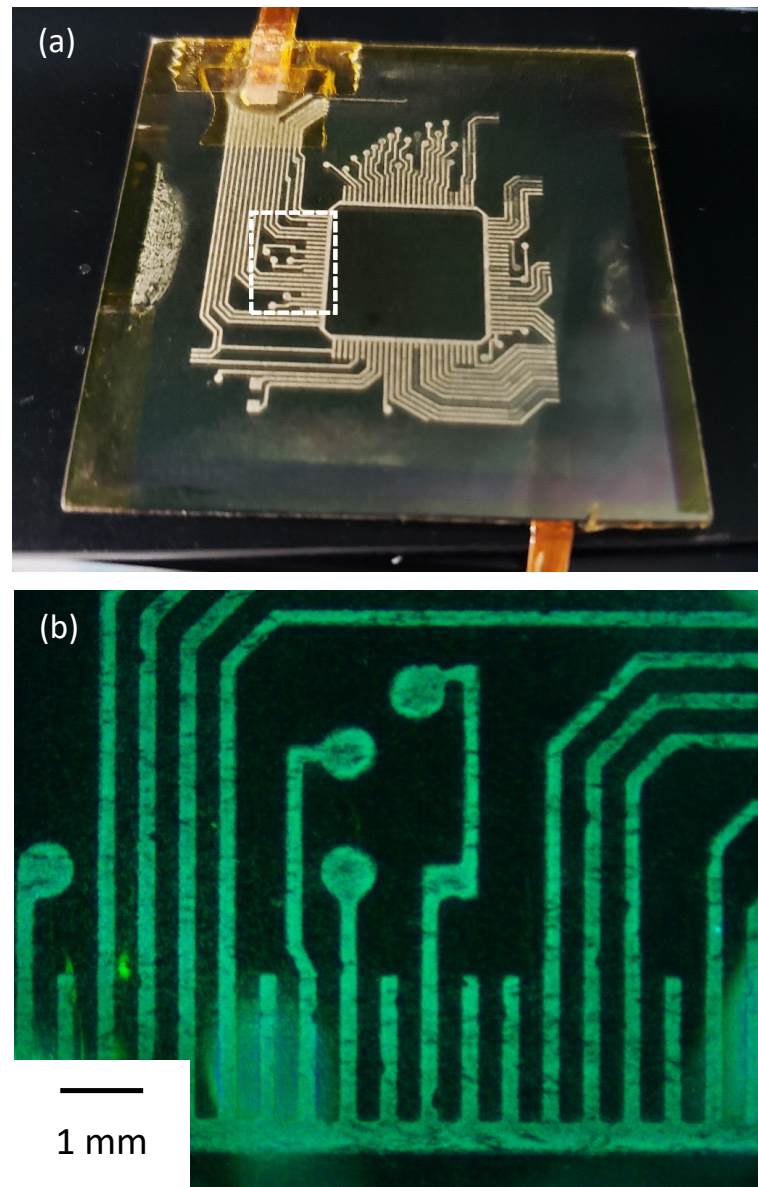


Figure 6. (a) Photograph of the Ag–Ni toner pattern formed with our toner printing method. (b) Optical micrograph of the Ag–Ni pattern indicated by the dashed rectangle in Figure 6a. The bright particles are the Ag–Ni particles.

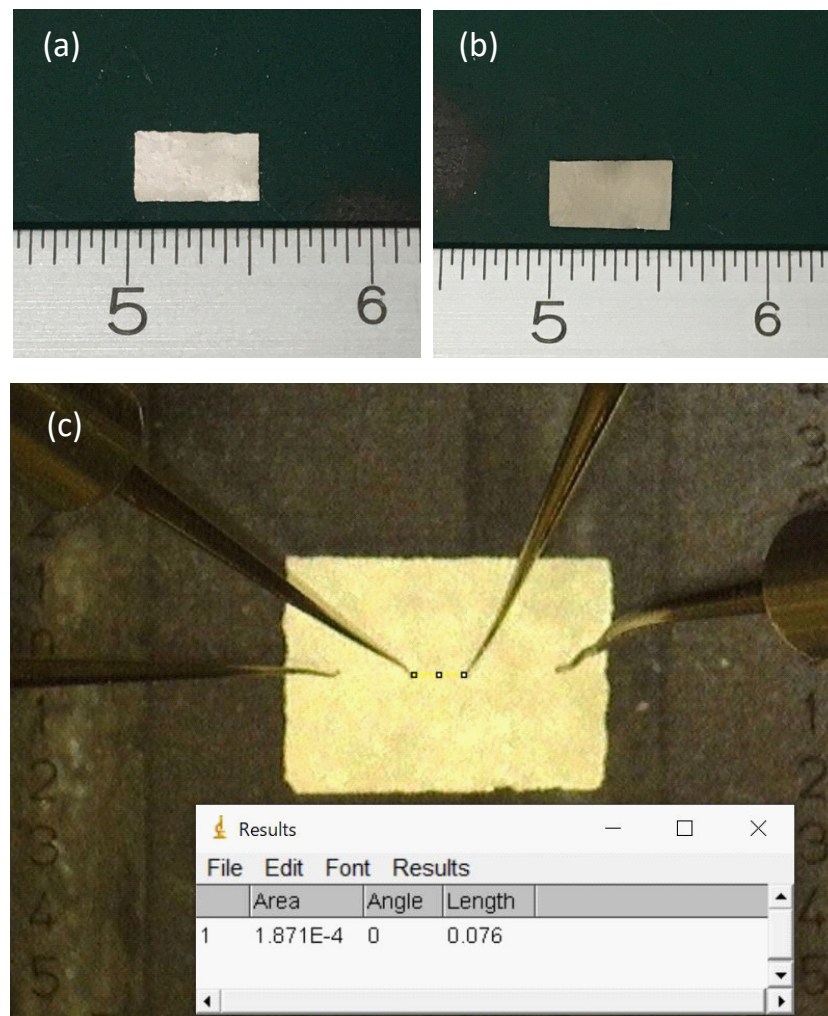


Figure 7. (a) Photograph of the compressed test piece; Ag toner particle. (b) Photograph of the compressed test piece; Ag-Ni toner particle. The electrical resistances were recorded using the 4-probe measurement, as shown in (c).

4. Conclusions

In this study, toner-type dry printing was proposed using Ag-Ni composite conductive toner particles, and the IC peripheral circuit was successfully patterned using the Ag-Ni toner. In addition, we demonstrated that the electrical resistivity of the compressed Ag-Ni piece was in the same range as that of bulk Ni. This value is sufficiently low for the electrical resistivity of the compressed powder. Our results indicate that the printing resolution is sufficient to create a printed circuit of current electronic products. Studies considering printing with higher resolutions, up to several μm , are currently in progress.

5. Patents

Japanese patent JP2021-150252 was obtained as a result of this study.

Author Contributions: Formal analysis and investigation, F.S., C.Y.N., R.H., K.K. and S.K.; resources, F.S.; Writing—original draft preparation, M.S. and F.S.; writing—review and editing, M.S. and C.Y.N.; supervision, K.K.; funding acquisition, K.K. and M.S. All authors have read and agreed to the published version of the manuscript.

Funding: This research was funded by a grant from the A-STEP program of the Japan Science and Technology Agency (number JPMJTM20CD).

Data Availability Statement: The data presented in this study are available upon request from the corresponding author.

Acknowledgments: The authors would like to thank T. Sawada of the RICHIO Company, Ltd., as well as H. Tomiya for the technical advice and experimental contributions, respectively.

Conflicts of Interest: The authors declare no conflict of interest. The funders had no role in the study design, collection, analyses, interpretation of data, writing of the manuscript, or decision to publish the results.

References

- Lu, B.H.; Lan, H.B.; Liu, H.Z. Additive manufacturing frontier: 3D printing electronics. *Opto-Electron Adv.* **2018**, *1*, 170004.
- Sevilla, G.A.T.; Cordero, M.D.; Nassar, J.M.; Hanna, A.N.; Kutbee, A.T.; Arevalo, A.; Hussain, M.M. Decal Electronics: Printable Packaged with 3D Printing High-Performance Flexible CMOS Electronic Systems. *Adv. Mater. Technol.* **2017**, *2*, 1600175.
- Mohammed, M.G.; Kramer, R. All-Printed Flexible and Stretchable Electronics. *Adv. Mater.* **2017**, *29*, 1604965.
- Khan, S.; Lorenzelli, L.; Dahiya, R.S. Technologies for Printing Sensors and Electronics Over Large Flexible Substrates: A Review. *IEEE Sens. J.* **2015**, *15*, 3164–3185.
- Vella, S.; Smithson, C.; Halfyard, K.; Shen, E.; Chretien, M. Integrated capacitive sensor devices aerosol jet printed on 3D objects. *Flex. Print. Electron.* **2019**, *4*, 045005.
- Ahmadi, Z.; Lee, S.; Patel, A.; Unocic, R.R.; Shamsaei, N.; Mahjouri-Samani, M. Dry Printing and Additive Nanomanufacturing of Flexible Hybrid Electronics and Sensors. *Adv. Mater. Interfaces* **2022**, *9*, 2102569.
- An B.W.; Kim, K.; Lee, H.; Kim, S.-Y.; Shim, Y.; Lee, D.-Y.; Song, J.Y.; Park, J.-U. High-Resolution Printing of 3D Structures Using an Electrohydrodynamic Ink-jet with Multiple Functional Inks. *Adv. Mater.* **2015**, *27*, 4322–4328.
- Shi, J.; Guo, C.X.; Chan-Park, M.B.; Li, C.M. All-Printed Carbon Nanotube finFETs on Plastic Substrates for High-Performance Flexible Electronics. *Adv. Mater.* **2012**, *24*, 358–361.
- Pace, G.; Grimaldi, A.; Natali, D.; Sampietro, M.; Coughlin, J.E.; Bazan, G.C.; Caironi, M. All-Organic and Fully-Printed Semitransparent Photodetectors Based on Narrow Bandgap Conjugated Molecules. *Adv. Mater.* **2014**, *26*, 6773–6777.
- Lee, C.; Kang, H.; Kim, H.; Nguyen, H.A.D.; Shin, K. Quality control with matching technology in roll to roll printed electronics. *J. Mech. Sci. Technol.* **2010**, *24*, 315–318.
- Yun, C.; Choi, J.; Kang, H.W.; Kim, M.; Moon, H.; Sung, H.J.; Yoo, S. Digital-Mode Organic Vapor-Jet Printing (D-OVJP): Advanced Jet-on-Demand Control of Organic Thin-Film Deposition. *Adv. Mater.* **2012**, *24*, 2857–2862.
- Guo, H.; Jiang, Z.; Ren, D.; Li, S.; Wang, J.; Cai, X.; Zhang, D.; Guo, Q.; Xiao, J.; Yang, J. High-Performance Flexible Micro-Supercapacitors Printed on Textiles for Powering Wearable Electronics. *ChemElectroChem* **2021**, *8*, 1574.
- Leenen, M.A.M.; Arning, V.; Thiem, H.; Steiger, J.; Anselmann, R. Printable electronics: Flexibility for the future. *Phys. Stat. Sol.* **2009**, *206*, 588–597.
- Janczak, D.; Zych, M.; Raczynski, T.; Dybowska-Sarapuk, L.; Peplowski, A.; Krzeminski, J.; Sosna-Glebska, A.; Znajdek, K.; Sibinski, M.; Jakubowska, M. Stretchable and Washable Electroluminescent Display Screen-Printed on Textile. *Nanomaterials* **2019**, *9*, 1276.
- Torres Sevilla, G.A.; Hussain, M.M. Printed Organic and Inorganic Electronics: Devices To Systems. *IEEE J. Emerg. Sel. Top. Circuits Syst.* **2017**, *7*, 147–160.
- Baker, D.V.; Bao, C.; Kim, W.S. Highly Conductive 3D Printable Materials for 3D Structural Electronics. *ACS Appl. Electron. Mater.* **2021**, *3*, 2423–2433.
- Li, W.; Li, F.; Li, H.; Su, M.; Gao, M.; Li, Y.; Su, D.; Zhang, X.; Song, Y. Flexible Circuits and Soft Actuators by Printing Assembly of Graphene. *ACS Appl. Mater. Interfaces* **2016**, *8*, 12369–12376.
- Jinsoo, N.; Minhun, J.; Kyunghwan, J.; Gwangyong, L.; Soyeon, L.; Daae, K.; Vivek, S.; Gyoujin, C. All Printed Edge-Triggered Register Using Single Walled Carbon Nanotube-Based Thin Film Transistor. *J. Nanosci. Nanotechnol.* **2012**, *12*, 4261–4264.
- Jansson, E.; Lyytikainen, J.; Tanninen, P.; Eiroma, K.; Leminen, V.; Immonen, K.; Hakola, L. Suitability of Paper-Based Substrates for Printed Electronics. *Materials* **2022**, *15*, 957.
- Frutiger, A.; Muth, J.T.; Vogt, D.M.; Menguc, Y.; Campo, A.; Valentine, A.D.; Walsh, C.J.; Lewis, J.A. Capacitive Soft Strain Sensors via Multicore-Shell Fiber Printing. *Adv. Mater.* **2015**, *27*, 2440–2446.
- Chung, S.; Jang, M.; Ji, S.-B.; Im, H.; Seong, N.; Ha, J.; Kwon, S.-K.; Kim, Y.-H.; Yang, H.; Hong, Y. Flexible High-Performance All-Inkjet-Printed Inverters: Organo-Compatible and Stable Interface Engineering. *Adv. Mater.* **2013**, *25*, 4773–4777.
- Wu, C.; Tetik, H.; Cheng, J.; Ding, W.; Guo, H.; Tao, X.; Zhou, N.; Zi, Y.; Wu, Z.; Wu, H.; et al. Electrohydrodynamic Jet Printing Driven by a Triboelectric Nanogenerator. *Adv. Funct. Mater.* **2019**, *29*, 1901102.
- Li, W.W.; Zhang, H.R.; Kagita, S.; Shamim, A. All Screen-Printed, Polymer-Nanowire Based Foldable Electronics for mm-Wave Applications. *Adv. Mater. Technol.* **2021**, *6*, 2100525.
- Bartzs, M.; Kempa, H.; Otto, M.; Hubler, A.; Zielke, D. Device and circuit simulation of printed polymer electronics. *Org. Electron.* **2007**, *8*, 431–438.
- Sung, D.; de la Fuente Vornbrock, A.; Subramanian, V. Scaling and Optimization of Gravure-Printed Silver Nanoparticle Lines for Printed Electronics. *IEEE Trans. Components Packag. Technol.* **2010**, *33*, 105–114.
- Roshanghias, A.; Krivec, M.; Baumgart, M. Sintering strategies for ink-jet printed metallic traces in 3D printed electronics. *Flex. Print. Electron.* **2017**, *2*, 045002.

27. Skarzynski, K.; Krzeminski, J.; Jakubowska, M.; Sloma, M. Highly conductive electronics circuits from aerosol jet printed silver inks. *Sci. Rep.* **2021**, *11*, 18141.
28. Lazarus, N.; Tsang, H.H. 3-D Printing Structural Electronics With Conductive Filaments. *IEEE Trans. Components Packag. Manuf. Technol.* **2020**, *10*, 1965–1972.
29. Feng, S.; Tian, Z.; Wang, J.; Cao, S.; Kong, D. Laser sintering of Zn microparticles and its application in printable biodegradable electronics. *Adv. Electron. Mater.* **2019**, *5*, 1800693.
30. Jiang, T.; Meng, X.; Zhou, Z.; Wu, Y.; Tian, Z.; Liu, Z.; Lu, G.; Eginlidil, M.; Yu, H.-D.; Liu, J.; et al. Highly flexible and degradable memory electronics comprised of all-biocompatible materials. *Nanoscale* **2021**, *13*, 724–729.
31. Shin, E.; Yoo, J.; Yoo, G.; Kim, Y.-J.; Kim, Y.S. Eco-friendly cross-linked polymeric dielectric material based on natural tannic acid. *Chem. Eng. J.* **2019**, *358*, 170–175.
32. Le, T.-S.D.; Lee, Y.A.; Nam, H.K.; Jang, K.Y.; Yang, D.; Kim, B.; Yim, K.; Kim, S.-W.; Yoon, H.; Kim, Y.-J. Green Flexible Graphene-Inorganic-Hybrid Micro-Supercapacitors Made of Fallen Leaves Enabled by Ultrafast Laser Pulses. *Adv. Funct. Mater.* **2022**, *32*, 2107768.
33. Horiuchi, Y.; Okada, Y.; Sakai, M.; Suzuki, M.; Tomiya, H. Solvent-free Printing of Organic Semiconductor, Insulator, Metal, and Conductor Particles on Flexible Substrates. *TechConnect Briefs* **2019**, *2019*, 361–364.
34. Sakai, M.; Koh, T.; Toyoshima, K.; Nakamori, K.; Okada, Y.; Yamauchi, H.; Sadamitsu, Y.; Shinamura, S.; Kudo, K. Solvent-Free Toner Printing of Organic Semiconductor Layer in Flexible Thin-Film Transistors. *Phys. Rev. Appl.* **2017**, *8*, 014001.
35. Rasband, W.S. *ImageJ*; U. S. National Institutes of Health: Bethesda, MD, USA, 1997–2012. Available online: <http://imagej.nih.gov/ij/> (accessed on 29 August 2022).
36. Schneider, C.A.; Rasb, W.S.; Eliceiri, K.W. NIH Image to ImageJ: 25 years of image analysis. *Nat. Methods* **2012**, *9*, 671–675.
37. Chen, C.; Suganuma, K. Microstructure and mechanical properties of sintered Ag particles with flake and spherical shape from nano to micro size. *Mater. Des.* **2019**, *162*, 311–321.
38. Chen, C.; Yeom, J.; Choe, C.; Liu, G.; Gao, Y.; Zhang, Z.; Zhang, B.; Kim, D.; Suganuma, K. Necking growth and mechanical properties of sintered Ag particles with different shapes under air and N₂ atmosphere. *J. Mater. Sci.* **2019**, *54*, 13344–13357.
39. Moon, K.S.; Dong, H.; Maric, R.; Pothukuchi, S.; Hunt, A.; Li, Y.; Wong, C.P. Thermal behavior of silver nanoparticles for low-temperature interconnect applications. *J. Electron. Mater.* **2005**, *34*, 168–175.
40. Jeong, J.-H.; Cho, T.-S. Sintering Behaviors of Ag Nanopowders with Different Particle Sizes: A Real-Time Synchrotron X-ray Scattering Study. *J. Nanosci. Nanotechnol.* **2017**, *17*, 7799–7803.
41. Yeom, J.; Nagao, S.; Chen, C.; Sugahara, T.; Zhang, H.; Choe, C.; Li, C.-F.; Suganuma, K. Ag particles for sinter bonding: Flakes or spheres? *Appl. Phys. Lett.* **2019**, *14*, 253103.
42. Ryu, K.; Moon, Y.J.; Park, K.; Hwang, J.-Y.; Moon, S.-J. Electrical Property and Surface Morphology of Silver Nanoparticles After Thermal Sintering. *J. Electron. Mater.* **2016**, *45*, 312–321.
43. Jiu, J.; Zhang, H.; Koga, S.; Nagao, S.; Izumi, Y.; Suganuma, K. Simultaneous synthesis of nano and micro-Ag particles and their application as a die-attachment material. *J. Mater. Sci. Mater. Electron.* **2015**, *26*, 7183–7191.
44. Lee, Y.-J.; Lee, J.-H. Effect of compression pressure on strength of low-temperature sinter bonding produced using silver formate. *Powder Metall.* **2021**, *64*, 235–240.
45. Fu, Y.Q.; Shearwood, C.; Xu, B.; Yu, L.G.; Khor, K.A. Characterization of spark plasma sintered Ag nanopowders. *Nanotechnology* **2010**, *21*, 115707.
46. Alarifi, H.A.; Ozdogan, C.; Hu, A.; Yavuz, M.; Zhou, Y. Molecular Dynamics Simulation of Sintering and Surface Premelting of Silver Nanoparticles. *Mater. Trans.* **2013**, *54*, 884–889.